Solvent effects in hyperpolarization of ^{15}N nuclei in [$^{15}N_3$]metronidazole and [$^{15}N_3$]nimorazole antibiotics via SABRE-SHEATH

Anna P. Yi,[a,b] Oleg G. Salnikov,*[a] Dudari B. Burueva,[a] Nikita V. Chukanov,[a] Eduard Y. Chekmenev,[c] and Igor V. Koptyug[a]

[a] A. P. Yi, Dr. O. G. Salnikov, Dr. D. B. Burueva, Dr. N. V. Chukanov, Prof. I. V. Koptyug
Laboratory of Magnetic Resonance Microimaging
International Tomography Center SB RAS
3A Institutskaya St., Novosibirsk 630090, Russia
E-mail: salnikov@tomo.nsc.ru

[b] A. P. Yi
Department of Natural Sciences
Novosibirsk State University
2 Pirogova St., Novosibirsk 630090, Russia

[c] Prof. E. Y. Chekmenev
Department of Chemistry, Integrative Bio-Sciences (IBIO), Karmanos Cancer Institute (KCI)
Wayne State University
Detroit, Michigan 48202, United States

Abstract: Metronidazole and nimorazole are antibiotics of a nitroimidazole group originally designed for acting on anaerobic bacteria. These antibiotics may be potentially utilized as hypoxia radiosensitizers for the treatment of cancerous tumors. Hyperpolarization of ^{15}N nuclei in these compounds using SABRE-SHEATH (Signal Amplification By Reversible Exchange in SHield Enables Alignment Transfer to Heteronuclei) approach provides dramatic enhancement of detection sensitivity of these analytes using magnetic resonance spectroscopy and imaging. Methanol-d_4 is conventionally employed as a solvent in SABRE hyperpolarization process. Herein, we investigate SABRE-SHEATH hyperpolarization of isotopically labeled [$^{15}N_3$]metronidazole and [$^{15}N_3$]nimorazole in nondeuterated methanol-h_4 and ethanol-h_6 solvents (with the latter one being more preferable for biomedical applications due to its significantly lower toxicity). Optimization of hyperpolarization parameters, such as polarization transfer magnetic field, temperature, parahydrogen flow rate and pressure, allowed us to obtain an average ^{15}N polarization of up to ca. 7.6% for both substrates. The highest ^{15}N polarizations were observed in methanol-d_4 for [$^{15}N_3$]metronidazole and in ethanol-h_6 for [$^{15}N_3$]nimorazole. At a clinically relevant magnetic field of 1.4 T the ^{15}N nuclei of these substrates possess long characteristic hyperpolarization lifetimes (T_1) in the range from ca. 1 to ca. 7 min, with the longest relaxation observed for $^{15}NO_2$ sites. This study represents a major step toward SABRE in more biocompatible solvents, such as ethanol, and also paves the way for future utilization of these hyperpolarized nitroimidazoles as molecular contrast agents for MRI visualization of tumors.

Introduction

Nuclear magnetic resonance (NMR) spectroscopy and magnetic resonance imaging (MRI) are widely used in a broad range of applications in chemistry, biology and medicine. However, both these techniques possess a significant limitation of intrinsically low sensitivity caused by small population difference of nuclear spin energy levels (i.e., small degree of nuclear spin polarization) at thermal equilibrium.[1] For example, at a clinically relevant magnetic field of 3 T and room temperature only a single ^1H nucleus out of every 100000 contributes to the observable NMR signal. For heteronuclei (e.g., ^{13}C or ^{15}N) the Boltzmann statistics is even less favorable considering the 4- and 10-times lower gyromagnetic ratio of these nuclei respectively compared to that of proton. Hyperpolarization techniques provide an efficient way to overcome this problem of low sensitivity by transiently creating non-equilibrium polarization of nuclear spins, allowing for enhancement of NMR signal up to several orders of magnitude.[2–4] Today, the main driver behind the development of hyperpolarization techniques is their possible application in a clinical setting for diagnostics of diseases with aberrant metabolism (especially in cancer).[5,6] In this context, hyperpolarization of heteronuclei is especially advantageous because of their longer relaxation times compared to protons, providing larger time window for administration of a hyperpolarized (HP) compound bolus to a patient, its uptake and MR sensing. Moreover, heteronuclei also exhibit greater chemical shift dispersion, allowing for easier discrimination of the introduced HP analyte and its downstream metabolites. Finally, in contrast to protons, there is virtually no background heteronuclear MR signal from tissues.[7]

Arguably, the most widespread technique suitable for hyperpolarization of heteronuclei is dissolution dynamic nuclear polarization (d-DNP),[8,9] based on the transfer of thermal polarization of a paramagnetic radical electron spins at low temperature and high magnetic field to nearby nuclear spins using microwave irradiation.[10,11]

D-DNP allows to hyperpolarize a wide range of metabolites,[12,13] for example, pyruvate,[14] glucose,[15] acetate,[16] fumarate,[17] α-ketoglutarate[18] etc. In spite of the successful translation of d-DNP from laboratory animal[14,19] to human[20] studies, its widespread clinical use is limited by the requirement of expensive (~$2M) and complex equipment and long polarization cycles (~1 h for producing a single dose of HP contrast agent).

Parahydrogen-induced polarization (PHIP)[21,22] and signal amplification by reversible exchange (SABRE)[23,24] techniques offer more affordable and high-throughput alternative to d-DNP.[25,26] Both of them employ singlet spin order of a parahydrogen (p-H_2) molecule as a source of hyperpolarization. Both techniques enable fast polarization time: generally, a bolus of HP contrast agent is prepared in ~1 min. In PHIP, p-H_2-derived H atoms are directly incorporated into the target HP molecule in a pairwise manner, i.e. two atoms from the same p-H_2 molecule end up in the same molecule of reaction product. SABRE relies on reversible binding of both p-H_2 and substrate molecules to an Ir complex accompanied by polarization transfer from p-H_2-derived hydrides to a coordinated target molecule via spin-spin couplings[27,28] (Figure 1). As a result of simultaneous chemical exchange, hyperpolarization is gradually accumulated on the free (i.e., uncoordinated) substrate.[23] SABRE enables hyperpolarization of a broad range of compounds,[27] e.g. various N-heterocycles,[23,29–31] nitriles,[32] amines,[33] and carboxylates.[34,35]

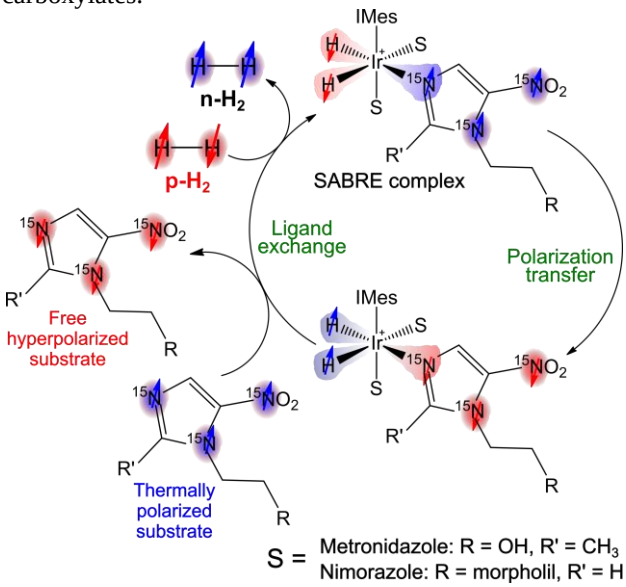

Figure 1. Scheme of the SABRE process. In the activated SABRE complex, polarization is transferred from p-H_2-derived hydrides to the substrate (S) molecule through a spin-relayed mechanism. Then normal (i.e., thermally polarized) hydrogen molecule (n-H_2) and hyperpolarized substrate are exchanged with p-H_2 and thermally polarized substrate, respectively, on the metal center.

Originally, SABRE approach was developed for hyperpolarization of protons,[23] and here it can provide impressive polarization levels of up to 50%.[36] However, as it was mentioned above, for prospective biomedical applications hyperpolarization of heteronuclei is needed. Transfer of SABRE polarization to heteronuclei is typically accomplished via one of the two approaches.[24,27] The first approach is based on the use of dedicated radiofrequency (RF) pulse sequences inside an NMR spectrometer at a high magnetic field, such as LIGHT-SABRE[37] or SLIC-SABRE.[38] The second approach called SABRE-SHEATH (SABRE in SHield Enables Alignment Transfer to Heteronuclei)[39,40] exploits bringing the system to an ultralow magnetic field in the range from hundreds of nanotesla to several microtesla. In this regime, level anti-crossing (LAC) conditions are fulfilled for the p-H_2-derived protons and to-be-hyperpolarized heteronuclei leading to polarization transfer between them.[27] To obtain microtesla fields, efficient shielding from the ambient magnetic field is required. Typically, SABRE-SHEATH allows to achieve greater polarization levels compared to high-field RF-based approaches, e.g. ^{15}N polarization (P_{15N}) of up to 9.8% for [^{15}N]pyridine using SABRE-SHEATH[39,40] vs. P_{15N} < 1% using SLIC-SABRE.[38,41] Another advantage of SABRE-SHEATH is its capability to hyperpolarize a wide range of substrates without the necessity to match experimental parameters for each compound individually.[42,43]

From the broad list of substrates amenable to SABRE-SHEATH polarization, the derivatives of nitroimidazole such as metronidazole,[44] nimorazole,[45] and ornidazole[46] are of particular interest. Because of their ability to be reduced in hypoxic conditions, these compounds are successfully utilized as antibiotics[47] or radiotracers in positron emission tomography (PET) imaging,[48] and have prospects for clinical utilization as hypoxia radiosensitizers,[49,50] (especially nimorazole which was under Phase 3 clinical study for the treatment of head and neck cancer).[51,52] Thus, hyperpolarized nitroimidazoles potentially can serve as molecular MRI contrast agents for hypoxic tumor visualization. Indeed, ^{15}N chemical shift dispersion of [$^{15}N_3$]nimorazole and [$^{15}N_3$]metronidazole and their putative metabolic products in hypoxic tissues is sufficient for the *in vivo* differentiation of these analytes to enable sensing of their uptake and metabolic transformation.[45,53] Thus, HP [$^{15}N_3$]nimorazole and [$^{15}N_3$]metronidazole have the potential to emerge as non-radioactive HP contrast agents of hypoxia sensing *in vivo*, in a manner similar to that of PET tracers, but with the advantages of employing no ionizing radiation and fast examination time (minutes versus hours). From the list of nitroimidazole antibiotics, metronidazole is the most well-studied as a target of SABRE hyperpolarization.[44,54–56] An impressive ^{15}N polarization level of 24% was achieved for metronidazole with natural abundance of ^{15}N isotope using SABRE-SHEATH,[44] with a further boost to P_{15N} = 54% via fine-tuning of Ir catalyst structure.[57] Isotopically labeled [$^{15}N_3$]metronidazole was efficiently hyperpolarized to P_{15N} of 10–16% for all three ^{15}N sites via spin-relayed polarization transfer mechanism.[54,55] Later, SABRE-SHEATH hyperpolarization of [$^{15}N_3$]nimorazole was also demonstrated albeit with lower P_{15N} levels of ca. 2–3%.[45] Importantly, the hyperpolarized state of $^{15}NO_2$ site in these compounds persisted for up to 20 minutes at 1.4 T field, with corresponding T_1 relaxation times of ca. 6–10 min.[45,54,55]

In these previous SABRE-SHEATH studies of isotopically enriched [$^{15}N_3$]metronidazole and

[$^{15}N_3$]nimorazole, methanol-d_4 was used as a solvent.[45,54,55] However, this it is a poor media choice for biomedical applications due to its toxicity and higher cost compared to nondeuterated solvents. Although previously Kiryutin et al. studied SABRE-SHEATH polarization of metronidazole in deuterated and nondeuterated methanol, ethanol, acetone and DMSO solvents,[56] in that work the substrate with natural abundance of ^{15}N nuclei was utilized, limiting the study mostly to metronidazole ^{15}N-3 site. Moreover, non-labeled metronidazole is not suitable for biomedical applications due to substantially reduced ^{15}N content.

Herein, we systematically investigate the impact of solvent nature and its deuteration on SABRE-SHEATH performance and hyperpolarization lifetimes of [$^{15}N_3$]metronidazole and [$^{15}N_3$]nimorazole. We utilize three alcohol solvents: CD_3OD, CH_3OH, and C_2H_5OH (the latter one being the most biocompatible). The use of isotopically labeled substrates enables tracking of all three ^{15}N sites in these compounds. Importantly, we were able to significantly improve the attainable P_{15N} levels for [$^{15}N_3$]nimorazole compared to previously published data,[45] and we show that both [$^{15}N_3$]metronidazole and [$^{15}N_3$]nimorazole can be polarized to the similar polarization levels (here – ca. 7.5% for each of the ^{15}N sites) provided that all experimental conditions are properly optimized.

Results and Discussion

SABRE-SHEATH experiments were performed using the MATRESHCA hyperpolarizer setup[58] allowing for variation of multiple experimental parameters (magnetic field, temperature, pressure, p-H_2 bubbling rate) in a reproducible way. The sample comprised a medium-wall 5 mm NMR tube containing 20 mM substrate ([$^{15}N_3$]metronidazole or [$^{15}N_3$]nimorazole) and 2 mM Ir precatalyst [Ir(IMes)(COD)Cl] in 0.5 mL of chosen solvent (CD_3OD, CH_3OH or C_2H_5OH). As the hours-long SABRE experiments lead to a gradual solvent evaporation, the additional saturator NMR tube with pure solvent was introduced in the fluid path before the sample tube.[59] ^{15}N NMR spectra were acquired on a 1.4 T SpinSolve Nitrogen 60 Ultra benchtop NMR spectrometer (Magritek). The example ^{15}N NMR spectra of SABRE-SHEATH-hyperpolarized [$^{15}N_3$]metronidazole and [$^{15}N_3$]nimorazole are presented in Figure 2.

First, the samples were activated via a continuous bubbling of p-H_2 through the solution at 20 standard cubic centimeters (sccm) gas flow rate until the attainable SABRE-SHEATH polarization approached a plateau. The SABRE-SHEATH activation process took from one to four hours depending on the substrate (Figure S3). The activation kinetics for [$^{15}N_3$]nimorazole in methanol-d_4 was in good agreement with the previously published data.[45] The slowest activation for both substrates was observed in CH_3OH, although the explanation of this fact demands further studies. Typically, SABRE activation process involves replacement of Cl and COD ligands by the substrate (S) molecules along with an oxidative addition of H_2, yielding [Ir(IMes)$(H)_2(S)_3$] SABRE-active complex.[60] Separately performed ^1H NMR studies showed that in the case of nimorazole substrate [Ir(IMes)$(H)_2(S)_3$] is indeed the major hydride species in solution (although NMR signal enhancement provided by high-field SABRE[61] revealed the presence of a number of minor hydride complexes, Figure S2). However, in the case of metronidazole a mixture of hydride complexes is formed, the major species likely being[62] [Ir(IMes)$(H)_2(S)_3$], [Ir(IMes)$(H)_2(S)_2Cl$], and [Ir(IMes)$(H)_2(S)_2(CD_3OD)$] (Figure S1). The difference between metronidazole and nimorazole in terms of the formed hydride complexes is likely attributed to steric constraints introduced by the presence of methyl group in metronidazole making [Ir(IMes)$(H)_2(S)_3$] complex less favorable compared to nimorazole and various pyridine derivatives.

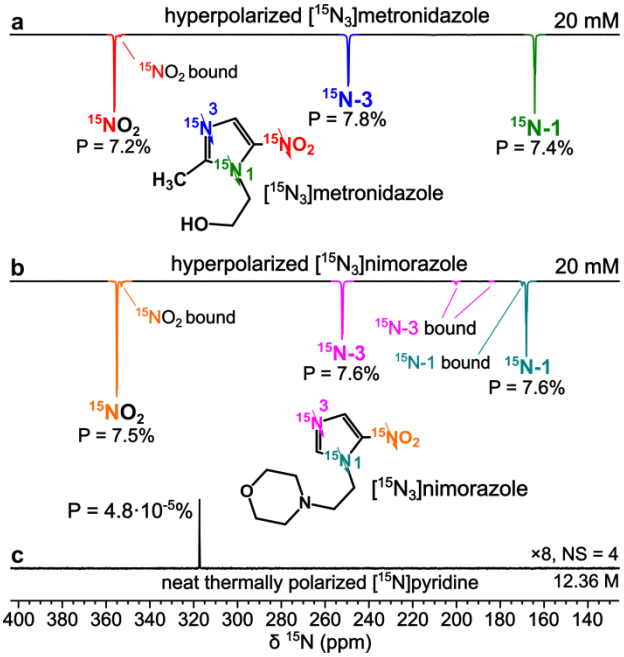

Figure 2. (a) ^{15}N NMR spectrum of HP [$^{15}N_3$]metronidazole in methanol-d_4 (SABRE-SHEATH hyperpolarization was performed at 23 °C and 0.70 μT). (b) ^{15}N NMR spectrum of HP [$^{15}N_3$]nimorazole in ethanol-h_6 (SABRE-SHEATH hyperpolarization was performed at 33 °C and 0.62 μT). (c) ^{15}N NMR spectrum of neat thermally polarized [^{15}N]pyridine acquired with 4 signal accumulations and multiplied by a factor of 8.

The key parameters of SABRE-SHEATH experiments are the polarization transfer field and the temperature. The effects of these parameters are strongly connected with each other, as explained in detail elsewhere.[56] In brief, the position of the maximum in magnetic field profile is determined by the width of the LAC rather than the position of the LAC itself. At the same time the width of the LAC depends on the active SABRE complex lifetime which is affected by temperature-controlled chemical exchange rates. Thus, the polarization transfer field and the temperature should be ideally optimized simultaneously. As the measurement of a full 2D map of ^{15}N SABRE-SHEATH polarization vs. these two parameters is time-consuming, here we started with the measurement of magnetic field profiles at four different temperatures with a 10 °C increment (from 13 to 43 °C for [$^{15}N_3$]metronidazole and from 23 to 53 °C for [$^{15}N_3$]nimorazole; the choice of temperature ranges was motivated by the previous

studies in methanol-d_4[45,55]). This allowed us to roughly identify the optimal temperature and precisely identify the corresponding optimized magnetic field which was then utilized for a precise measurement of the temperature profile. The obtained polarization transfer field and temperature profiles for [$^{15}N_3$]metronidazole and [$^{15}N_3$]nimorazole in methanol-h_4 and ethanol-h_6 are presented in Figure 3. For [$^{15}N_3$]metronidazole, the maximal ^{15}N polarization was observed at ~22 °C and 0.70 μT in methanol-h_4 (Figure 3a,b) and at ~20 °C and 0.70 μT in ethanol-h_6 (Figure 3c,d). The optimal parameters for [$^{15}N_3$]nimorazole were 43 °C and 0.55 μT in methanol-h_4 (Figure 3e,f) and 34 °C and 0.62 μT in ethanol-h_6 (Figure 3g,h).

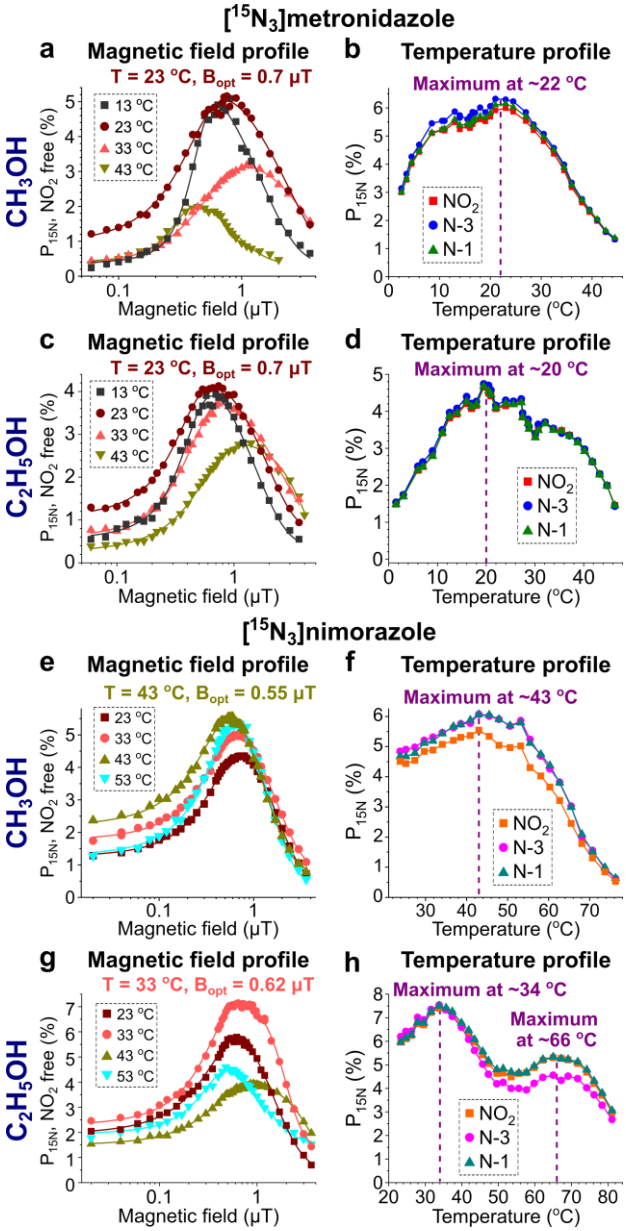

Figure 3. Magnetic field and temperature profiles of SABRE-SHEATH ^{15}N hyperpolarization of [$^{15}N_3$]metronidazole and [$^{15}N_3$]nimorazole in nondeuterated solvents: (a) Magnetic field profiles of P_{15N} of free [$^{15}N_3$]metronidazole $^{15}NO_2$ nuclei at four different temperatures in methanol-h_4. (b) Temperature profiles of P_{15N} of free [$^{15}N_3$]metronidazole ^{15}N nuclei in methanol-h_4 hyperpolarized at 0.70 μT. (c) Magnetic field profiles of P_{15N} of free [$^{15}N_3$]metronidazole $^{15}NO_2$ nuclei at four different temperatures in ethanol-h_6. (d) Temperature profiles of P_{15N} of free [$^{15}N_3$]metronidazole ^{15}N nuclei in ethanol-h_6 hyperpolarized at 0.70 μT. (e) Magnetic field profiles of P_{15N} of free [$^{15}N_3$]nimorazole $^{15}NO_2$ nuclei at four different temperatures in methanol-h_4. (f) Temperature profiles of P_{15N} of free [$^{15}N_3$]nimorazole ^{15}N nuclei in methanol-h_4 hyperpolarized at 0.55 μT. (g) Magnetic field profiles of P_{15N} of free [$^{15}N_3$]nimorazole $^{15}NO_2$ nuclei at four different temperatures in ethanol-h_6. (h) Temperature profiles of P_{15N} of free [$^{15}N_3$]nimorazole ^{15}N nuclei in ethanol-h_6 hyperpolarized at 0.62 μT. All measurements were performed at 70 sccm gas flow rate and 7.8 bar p-H_2 pressure.

The maxima in magnetic field profiles for solutions in methanol-d_4 were at the same positions as in the case of other solvents (in particular, 0.70 μT for [$^{15}N_3$]metronidazole and 0.58 μT for [$^{15}N_3$]nimorazole, Figure S4). Each combination of substrate and solvent provided approximately the same positions of the maxima in the magnetic field profiles for all ^{15}N sites for the free substrates and for the substrates coordinated in equatorial and axial positions (Figure S4), proving the spin-relayed mechanism of polarization transfer.[63] The obtained optimal temperatures of ca. 20–23 °C for [$^{15}N_3$]metronidazole are in excellent agreement with the previously published data for methanol-d_4 solutions.[55] As for [$^{15}N_3$]nimorazole, the previous study by some of us established the optimal temperature for SABRE-SHEATH in methanol-d_4 as 54 °C,[45] while here the maxima were observed at lower temperatures of 43 °C for methanol-h_4 and 34 °C for ethanol-h_6. This difference is likely attributed not to the change of solvent but rather to the use of lower concentrations (2.5 times lower catalyst concentration and 5 times lower substrate concentration were used here compared to the earlier study[45]). Also we note that the MATRESHCA setup[58] used here allowed for more accurate temperature sweep measurements compared to the protocol used in the previous study.[45] Interestingly, the temperature profile for [$^{15}N_3$]nimorazole in ethanol revealed the second local maximum at ca. 66 °C. This result may be explained by the fact that there are two simultaneous chemical exchange processes undergoing in SABRE, namely substrate exchange and p-H_2 exchange. Each of them may be optimized at different temperatures leading to the observation of two maxima in the SABRE-SHEATH temperature profile. This hypothesis is additionally confirmed by the fact that hyperpolarization of axial [$^{15}N_3$]metronidazole and [$^{15}N_3$]nimorazole substrates is optimized at higher temperatures compared to free and equatorial substrates (Figure S5). As the axial substrates typically do not dissociate,[64] their polarization is likely governed by p-H_2 exchange only (besides the spin dynamics factors). Unfortunately, the measurement of exchange kinetics was found to be problematic for both substrates due to an overlap of corresponding ^1H NMR signals (see Figure S11). For metronidazole, ^1H chemical shifts of the aromatic proton of free and equatorial substrate are separated only by 0.02 ppm at –30 °C and are totally indistinguishable at room temperature, making it impossible to use EXSY approach to measure the exchange rates. For nimorazole, ^1H NMR signals of two non-equivalent aromatic protons at C-2 and C-4 atoms overlap with each other, despite a better separation of signals of free and equatorial substrate (by ca. 0.1 and ca.

0.5 ppm for these two aromatic protons). Moreover, the signal of the α-CH_2 group of nimorazole sidearm overlaps with the signal of orthohydrogen. As a result, the standard EXSY approach is not suitable to measure the substrate and hydrogen exchange rates for the Ir complexes with these two nitroimidazole compounds.

Next, the dependences of SABRE-SHEATH ^{15}N polarization on p-H_2 flow rate were investigated. Typically, P_{15N} increased monotonously, eventually reaching a plateau at the flow rates of ca. 70 sccm (Figure S6). However, for [$^{15}N_3$]nimorazole in methanol-h_4 the polarization dependence on the p-H_2 flow rate showed a maximum at approximately 80 sccm followed by polarization decrease at higher flow rates. This anomalous behavior may be tentatively related to the fact that in methanol-h_4 [$^{15}N_3$]nimorazole was hyperpolarized at the higher temperature of 43 °C, which may affect gas/liquid diffusion, bubble sizes, capillary effects etc., finally affecting the rate of p-H_2 refreshment in solution. Polarization dependence on the p-H_2 pressure typically showed a monotonous growth rationalized by higher solubility of hydrogen at higher pressures (Figure S7). However, in the case of [$^{15}N_3$]metronidazole in ethanol-h_6 polarization reached a maximum at ca. 3.5 bar with a subsequent slight decline. This result may be tentatively explained by the assumption that at high pressure the hydrogen exchange becomes too fast to ensure efficient polarization transfer from the hydrides to the ^{15}N nuclei for this substrate/solvent system (although it should be noted that pressure also affects the volumetric flow rate because these measurements were performed under a constant mass flow rate; thus, the impact of pressure and p-H_2 bubbling rate cannot be easily rationalized).

Next, ^{15}N polarization buildup and decay kinetics in microtesla magnetic fields were investigated. Polarization buildup was measured by varying p-H_2 bubbling duration, while polarization decay was measured by keeping the sample inside the magnetic shield for a variable time after cessation of gas bubbling. These measurements were performed under previously optimized polarization transfer fields and temperatures: 0.70 μT and 23 °C for [$^{15}N_3$]metronidazole in all solvents, 0.55 μT and 43 °C for [$^{15}N_3$]nimorazole in methanol-d_4 and methanol-h_4 and 0.62 μT and 33 °C for [$^{15}N_3$]nimorazole in ethanol-h_6. The corresponding polarization buildup and decay curves are presented in Figures S8 and S9, while the fitted polarization buildup (T_b) and decay (T_1) exponential time constants are presented in Table 1. In SABRE-SHEATH experiments, polarization is accumulated in the pool of free substrate molecules during p-H_2 bubbling until the rates of polarization buildup (resulting from supply of fresh p-H_2 in the solution, polarization transfer and ligands exchange) and decay (resulting from relaxation effects) become equal to each other, establishing a plateau. The obtained results demonstrate that T_b and T_1 values for a chosen set of substrate, solvent and ^{15}N site are comparable, confirming the trend observed in earlier studies.[45,55] This fact can be rationalized using a simple kinetic analysis in the case when relaxation rate constant is significantly greater than the apparent hyperpolarization rate constant (see SI). Faster relaxation of the ^{15}N-3 sites compared to $^{15}NO_2$ and ^{15}N-1 sites is clearly due to the fact that ^{15}N-3 sites coordinate to Ir center of the polarization transfer catalyst. As for the solvent effects on relaxation kinetics at microtesla fields, the longest T_1 times for [$^{15}N_3$]metronidazole were observed in methanol-h_4. In the case of [$^{15}N_3$]nimorazole, both nondeuterated solvents provided similar relaxation times which were greater than those in methanol-d_4. The T_b and T_1 values for free and equatorial substrate molecules were close to each other, reflecting an efficient averaging of these values due to substrate exchange (Tables S7 and S8). On the other hand, ^{15}N nuclei of non-exchangeable axial substrates clearly showed longer buildup and relaxation times compared to those of free and equatorial substrates.

Table 1. ^{15}N SABRE-SHEATH polarization buildup (T_b) and decay (T_1) times for ^{15}N nuclei of free [$^{15}N_3$]metronidazole and [$^{15}N_3$]nimorazole in methanol-d_4, methanol-h_4 and ethanol-h_6 at optimized microtesla fields and temperatures.

Substrate	Solvent	T_b (s)			T_1 (s)		
		$^{15}NO_2$	^{15}N-3	^{15}N-1	$^{15}NO_2$	^{15}N-3	^{15}N-1
[$^{15}N_3$]metronidazole	CD_3OD	14 ± 1	6.9 ± 0.4	11.6 ± 0.7	16.3 ± 0.3	11.7 ± 0.6	15.2 ± 0.2
	CH_3OH	27.0 ± 0.7	16.6 ± 0.9	23.8 ± 0.4	25 ± 1	17.5 ± 0.8	23.1 ± 0.7
	C_2H_5OH	13.7 ± 0.7	10.2 ± 0.8	13.0 ± 0.6	9.9 ± 0.1	8.2 ± 0.5	9.5 ± 0.2
[$^{15}N_3$]nimorazole	CD_3OD	9.4 ± 0.4	5.2 ± 0.3	6.9 ± 0.2	8.2 ± 0.1	5.9 ± 0.3	7.0 ± 0.2
	CH_3OH	12.8 ± 0.6	7.0 ± 0.7	9.6 ± 0.5	13.1 ± 0.5	9.5 ± 0.3	11.3 ± 0.1
	C_2H_5OH	15.6 ± 0.9	9.4 ± 0.6	12.9 ± 0.4	13.1 ± 0.6	8.8 ± 0.1	11.3 ± 0.2

The hyperpolarized states of nitroimidazoles ^{15}N nuclei are known to persist for relatively long time of several minutes at a high magnetic field in the range from hundreds millitesla to several tesla.[45,55,56] In this work we used the 1.4 T magnetic field of a benchtop NMR spectrometer for high-field relaxation measurements. Importantly, 1.4 T is close to the typical magnetic fields of clinical MRI scanners. The obtained decay curves along with the corresponding T_1 relaxation times are shown in Figure 4. In agreement with previous studies,[45,54,55] the longest relaxation was observed for the $^{15}NO_2$ sites. For the [$^{15}N_3$]metronidazole $^{15}NO_2$ and ^{15}N-1 sites, the longest decay times were observed in methanol-h_4 (413 ± 7 s and 196 ± 2 s, respectively), while for the ^{15}N-3 site the longest decay was obtained in methanol-d_4 (220 ± 8 s). For [$^{15}N_3$]nimorazole the $^{15}NO_2$ site showed the highest T_1 in methanol-d_4 (349 ± 8) while for the ^{15}N-3 and ^{15}N-1 sites the longest relaxation was observed in methanol-h_4 (101 ± 1 s and 122 ± 2 s, respectively). The measured relaxation times for [$^{15}N_3$]nimorazole in methanol-d_4 at 1.4 T were in excellent agreement with previously published results.[45] Because the nitro group of nitroimidazoles is subjected to reduction *in vivo*,[65] the lifetime of HP ^{15}N-3 and ^{15}N-1

sites may eventually be more important for prospective biomedical applications of these compounds than the hyperpolarization lifetime of the $^{15}NO_2$ group. The previously calculated ^{15}N chemical shifts of three ^{15}N sites in [$^{15}N_3$]metronidazole, [$^{15}N_3$]nimorazole and their putative metabolic products in hypoxic tissues indicate that any of these sites may be suitable for tracking nitroimidazoles metabolism *in vivo*.[45,53]

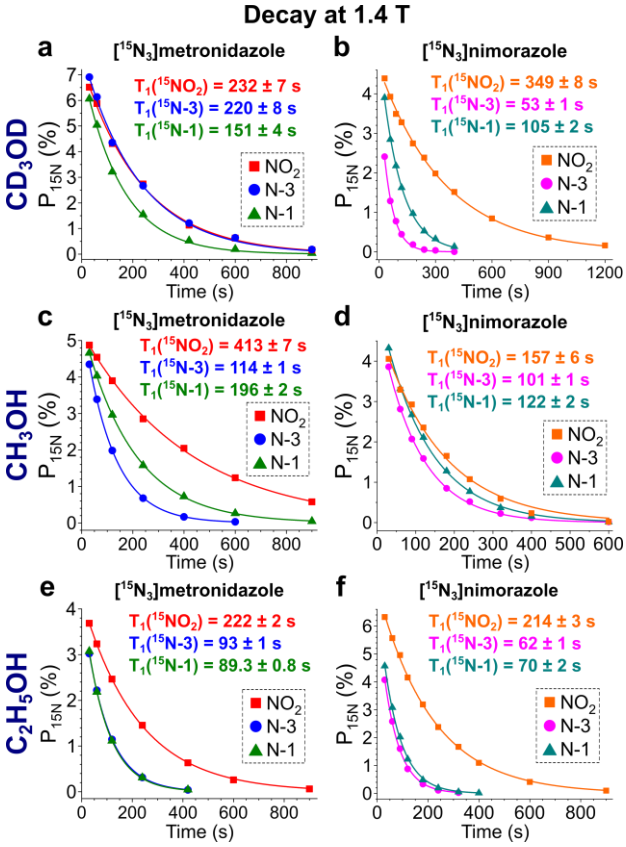

Figure 4. ^{15}N SABRE-SHEATH polarization decay kinetics at 1.4 T for: (a) [$^{15}N_3$]metronidazole in methanol-d_4, (b) [$^{15}N_3$]nimorazole in methanol-d_4, (c) [$^{15}N_3$]metronidazole in methanol-h_4, (d) [$^{15}N_3$]nimorazole in methanol-h_4, (e) [$^{15}N_3$]metronidazole in ethanol-h_6, (f) [$^{15}N_3$]nimorazole in ethanol-h_6. All measurements were performed for the samples hyperpolarized at 70 sccm gas flow rate and 7.8 bar p-H_2 pressure at the optimized temperature and polarization transfer field.

The highest polarization levels obtained for ^{15}N nuclei of [$^{15}N_3$]metronidazole and [$^{15}N_3$]nimorazole in the three solvents used in this study are shown in Figure 5. For [$^{15}N_3$]metronidazole, the maximal attainable polarization decreased from CD_3OD ($P_{15N,max}$ = 7.6%) to CH_3OH ($P_{15N,max}$ = 6.1%) and then to C_2H_5OH ($P_{15N,max}$ = 4.7%) (the values averaged across the three ^{15}N sites are presented here). For [$^{15}N_3$]nimorazole, the highest polarizations were observed in ethanol-h_6 ($P_{15N,max}$ = 7.65%), while methanol-h_4 and methanol-d_4 provided similar polarization levels ($P_{15N,max}$ of 6.1% and 5.8%, respectively). Thus, we show that careful optimization of experimental conditions allows one to achieve similar polarization levels for both [$^{15}N_3$]metronidazole and [$^{15}N_3$]nimorazole substrates. Moreover, the 7.65% ^{15}N polarization of [$^{15}N_3$]nimorazole demonstrated here is ca. 3 times greater than the previously reported values.[45]

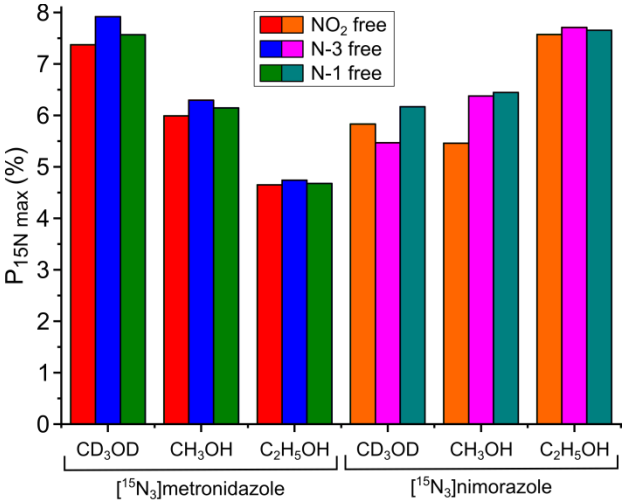

Figure 5. The histogram of maximum ^{15}N polarization values for free [$^{15}N_3$]metronidazole (left panel) and [$^{15}N_3$]nimorazole (right panel) at optimized conditions in methanol-d_4, methanol-h_4 and ethanol-h_6.

Conclusions

In this work, SABRE-SHEATH hyperpolarization of [$^{15}N_3$]metronidazole and [$^{15}N_3$]nimorazole in three alcohol solvents (methanol-d_4, methanol-h_4 and ethanol-h_6) was investigated. Magnetic field profiles at variable temperatures and temperature profiles at a fixed magnetic field were measured, allowing to identify the optimal conditions for SABRE-SHEATH hyperpolarization. While for [$^{15}N_3$]metronidazole ^{15}N polarization was maximized at ca. 23 °C and 0.70 μT in all three solvents, for [$^{15}N_3$]nimorazole the optimal conditions were achieved at higher temperatures and lower magnetic fields (43 °C and 0.55 μT for methanol-h_4 and 33 °C and 0.62 μT for ethanol-h_6). The effects of p-H_2 flow rate and pressure on the attainable polarizations were also studied. At the clinically relevant magnetic field of 1.4 T, $^{15}NO_2$ sites showed long T_1 relaxation times of several minutes, allowing to detect the HP ^{15}N signal even 20 minutes after the SABRE-SHEATH hyperpolarization process. In particular, [$^{15}N_3$]metronidazole nitro group exhibited T_1 of 6.9 ± 0.1 min in CH_3OH, and [$^{15}N_3$]nimorazole nitro group had T_1 of 5.8 ± 0.1 min in CD_3OD. The two other ^{15}N-3 and ^{15}N-1 sites relaxed faster, but nevertheless the corresponding T_1 values were rather high (from ca. 1 to ca. 3.5 min). Comparing polarization levels in the three solvents under study, the greatest values for [$^{15}N_3$]metronidazole were observed in methanol-d_4 and for [$^{15}N_3$]nimorazole in ethanol-h_6 ($P_{15N,max} \approx$ 7.6% for both compounds). Optimization of SABRE-SHEATH hyperpolarization in nondeuterated solvents is an important step for possible *in vivo* applications of hyperpolarized metronidazole and nimorazole. The obtained high polarization levels and fairly long hyperpolarization lifetimes of these compounds demonstrate great prospects for their possible application as molecular MRI contrast agents reporting on hypoxia status of cancerous tumors.

Experimental Section

[$^{15}N_3$]metronidazole and [$^{15}N_3$]nimorazole were synthesized according to the procedures described earlier.[45,54] The SABRE precatalyst [Ir(IMes)(COD)Cl] (IMes = 1,3-dimesitylimidazol-2-ylidene, COD = 1,5-cyclooctadiene) was synthesized according to the previously published procedure.[66] Ethanol and methanol were stored over 4 Å molecular sieves. Methanol-d_4 (Zeotope, 99.8% D) was handled in a glove box under argon atmosphere (molecular sieves were not used here because they promote H/D exchange in the solvent molecules). Ultrapure hydrogen gas was enriched with p-H_2 using parahydrogen generator based on a closed-cycle helium cryostat (CryoPribor, CFA-200-H2CELL) and a cryocompressor (Sumitomo, Zephyr HC-4A). Hydrated iron oxide FeO(OH) (Sigma-Aldrich, 371254) was used in a cell as a spin conversion catalyst. The enrichment of p-H_2 was 94% according to gas phase NMR spectra quantification. For SABRE-SHEATH experiments, the MATRESHCA hyperpolarizer setup was employed which was described in detail elsewhere.[58] A benchtop SpinSolve Nitrogen 60 Ultra NMR spectrometer (Magritek, New Zealand) with 1.4 T field was utilized for NMR spectra acquisition.

A 0.5 mL of solution containing 2 mM Ir precatalyst and 20 mM nitroimidazole substrate was transferred into a 5 mm medium-wall NMR tube tightly connected with a 1/4 in. outer diameter (OD) PTFE tube. Approximately 1 mL of pure solvent (methanol-d_4, methanol-h_4 or ethanol-h_6) was places in a 5 mm high-throughput NMR tube ("saturator tube") also tightly connected with a 1/4 in. OD PTFE tube. All p-H_2 supply lines before the sample NMR tube were made from 1/8 in. OD PEEK tubing except the 0.6 mm OD (0.3 mm inner diameter) PTFE catheter used to bubble p-H_2 into the solution in the sample tube. This thin catheter was chosen to minimize the magnetic field inhomogeneities inside the sample. The fluid path of the MATRESHCA hyperpolarizer setup (see Figure S12) was purged with p-H_2 for several minutes. Next, both the saturator and the sample NMR tubes were connected to the setup. After the fluid path was pressurized with p-H_2 to 7.8 bar, the activation of the sample was initiated via bubbling p-H_2 through both NMR tubes at 20 standard cubic centimeters per minute (sccm) flow rate and room temperature (23 °C). The gas flow rate was regulated using a mass flow controller (SmartTrak 50, Sierra Instruments, Monterey, CA, USA). During activation the sample was kept in a degaussed three-layered MuMETAL shield (Magnetic Shield Corp., Bensenville, IL, USA, P/N ZG-203) with a solenoid magnet inside allowing for precise control of the microtesla magnetic field inside the shield (0.70 μT for [$^{15}N_3$]metronidazole and 0.60 μT for [$^{15}N_3$]nimorazole). A resistor bank (Global Specialties, RDB-10) was employed to attenuate the DC current of the power supply unit to achieve the desirable value of the magnetic field inside the shield. SABRE-SHEATH process activation was monitored by recording ^{15}N NMR spectra of hyperpolarized solutions every 5–10 minutes (for this, p-H_2 bubbling through the solution was terminated by opening the bypass valve and the sample was manually transferred to the NMR spectrometer). After ^{15}N polarization reached a plateau, the desired measurements were performed. When required, the sample temperature was increased using a heating system consisting of a water circulation circuit, a heater and a PID-controller (described in detail elsewhere[58]) or decreased using an ice-water bath. In the pressure sweep experiments, a 100-psi safety valve (keeping the pressure at 100 psig, i.e. 7.8 bar) was replaced by a Swagelok membrane back pressure regulator (KBP Series). The measurements of polarization buildup kinetics were carried out by varying the duration of p-H_2 bubbling through the sample at the microtesla magnetic field. The microtesla polarization decay kinetics were measured by introducing a variable delay between the cessation of p-H_2 bubbling and moving the sample out of the magnetic shield. Polarization decays at 1.4 T were measured using a variable delay between the placement of the sample inside the NMR spectrometer and the start of an NMR signal acquisition. Unless stated otherwise, the experiments were done at the following typical conditions (polarization transfer magnetic field and temperature): 0.70 μT and 23 °C for [$^{15}N_3$]metronidazole in all solvents, 0.62 μT and 33 °C for [$^{15}N_3$]nimorazole in ethanol-h_6, 0.55 μT and 43 °C for [$^{15}N_3$]nimorazole in methanol-h_4 and methanol-d_4. The pressure of p-H_2 was 7.8 bar (100 psig), and its flow rate was 70 sccm.

Acknowledgements

A.P.Y., O.G.S., D.B.B. and N.V.C. thank the Russian Science Foundation (grant 21-73-10105). E.Y.C. thanks NSF CHE-1904780 and NIBIB R21 EB033872.

Conflict of Interest

E.Y.C. declares a stake of ownership in XeUS Technologies, LTD. Also E.Y.C. holds stock of Vizma Life Sciences (VLS) and serves on the scientific advisory board (SAB) of VLS.

Keywords: NMR spectroscopy • parahydrogen • hyperpolarization • SABRE • metronidazole • nimorazole

References

[1] J.-H. Ardenkjaer-Larsen, G. S. Boebinger, A. Comment, S. Duckett, A. S. Edison, F. Engelke, C. Griesinger, R. G. Griffin, C. Hilty, H. Maeda, G. Parigi, T. Prisner, E. Ravera, J. van Bentum, S. Vega, A. Webb, C. Luchinat, H. Schwalbe, L. Frydman, *Angew. Chem., Int. Ed.* **2015**, *54*, 9162–9185.

[2] J. Eills, D. Budker, S. Cavagnero, E. Y. Chekmenev, S. J. Elliott, S. Jannin, A. Lesage, J. Matysik, T. Meersmann, T. Prisner, J. A. Reimer, H. Yang, I. V. Koptyug, *Chem. Rev.* **2023**, *123*, 1417–1551.

[3] K. V. Kovtunov, E. V. Pokochueva, O. G. Salnikov, S. F. Cousin, D. Kurzbach, B. Vuichoud, S. Jannin, E. Y. Chekmenev, B. M. Goodson, D. A. Barskiy, I. V. Koptyug, *Chem. – An Asian J.* **2018**, *13*, 1857–1871.

[4] P. Nikolaou, B. M. Goodson, E. Y. Chekmenev, *Chem. – A Eur. J.* **2015**, *21*, 3156–3166.

[5] J. Kurhanewicz, D. B. Vigneron, J. H. Ardenkjaer-Larsen, J. A. Bankson, K. Brindle, C. H. Cunningham, F. A. Gallagher, K. R. Keshari, A. Kjaer, C. Laustsen, D. A. Mankoff, M. E. Merritt, S. J. Nelson, J. M. Pauly, P. Lee, S. Ronen, D. J. Tyler, S. S. Rajan, D. M. Spielman, L. Wald, X. Zhang, C. R. Malloy, R. Rizi,

Neoplasia **2019**, *21*, 1–16.
[6] J. Kurhanewicz, D. B. Vigneron, K. Brindle, E. Y. Chekmenev, A. Comment, C. H. Cunningham, R. J. DeBerardinis, G. G. Green, M. O. Leach, S. S. Rajan, R. R. Rizi, B. D. Ross, W. S. Warren, C. R. Malloy, *Neoplasia* **2011**, *13*, 81–97.
[7] D. L. Rothman, H. M. De Feyter, R. A. de Graaf, G. F. Mason, K. L. Behar, *NMR Biomed.* **2011**, *24*, 943–957.
[8] J. H. Ardenkjaer-Larsen, *J. Magn. Reson.* **2016**, *264*, 3–12.
[9] J. H. Ardenkjær-Larsen, B. Fridlund, A. Gram, G. Hansson, L. Hansson, M. H. Lerche, R. Servin, M. Thaning, K. Golman, *Proc. Natl. Acad. Sci. U. S. A.* **2003**, *100*, 10158–10163.
[10] S. J. Elliott, Q. Stern, M. Ceillier, T. El Daraï, S. F. Cousin, O. Cala, S. Jannin, *Prog. Nucl. Magn. Reson. Spectrosc.* **2021**, *126–127*, 59–100.
[11] A. C. Pinon, A. Capozzi, J. H. Ardenkjær-Larsen, *Magn. Reson. Mater. Phys., Biol. Med.* **2021**, *34*, 5–23.
[12] Y. Kondo, H. Nonaka, Y. Takakusagi, S. Sando, *Angew. Chem., Int. Ed.* **2021**, *60*, 14779–14799.
[13] K. R. Keshari, D. M. Wilson, *Chem. Soc. Rev.* **2014**, *43*, 1627–59.
[14] K. Golman, R. in 't Zandt, M. Thaning, *Proc. Natl. Acad. Sci. U. S. A.* **2006**, *103*, 11270–11275.
[15] M. Mishkovsky, B. Anderson, M. Karlsson, M. H. Lerche, A. D. Sherry, R. Gruetter, Z. Kovacs, A. Comment, *Sci. Rep.* **2017**, *7*, 11719.
[16] J. A. M. Bastiaansen, T. Cheng, M. Mishkovsky, J. M. N. Duarte, A. Comment, R. Gruetter, *Biochim. Biophys. Acta* **2013**, *1830*, 4171–4178.
[17] F. A. Gallagher, M. I. Kettunen, D.-E. Hu, P. R. Jensen, R. in 't Zandt, M. Karlsson, A. Gisselsson, S. K. Nelson, T. H. Witney, S. E. Bohndiek, G. Hansson, T. Peitersen, M. H. Lerche, K. M. Brindle, *Proc. Natl. Acad. Sci. U. S. A.* **2009**, *106*, 19801–19806.
[18] M. Mishkovsky, A. Comment, R. Gruetter, *J. Cereb. Blood Flow Metab.* **2012**, *32*, 2108–2113.
[19] K. Golman, R. in't Zandt, M. Lerche, R. Pehrson, J. H. Ardenkjaer-Larsen, *Cancer Res.* **2006**, *66*, 10855–10860.
[20] S. J. Nelson, J. Kurhanewicz, D. B. Vigneron, P. E. Z. Larson, A. L. Harzstark, M. Ferrone, M. van Criekinge, J. W. Chang, R. Bok, I. Park, G. Reed, L. Carvajal, E. J. Small, P. Munster, V. K. Weinberg, J. H. Ardenkjaer-larsen, A. P. Chen, R. E. Hurd, L.-I. Odegardstuen, F. J. Robb, J. Tropp, J. A. Murray, *Sci. Transl. Med.* **2013**, *5*, 198ra108.
[21] C. R. Bowers, D. P. Weitekamp, *J. Am. Chem. Soc.* **1987**, *109*, 5541–5542.
[22] T. C. Eisenschmid, R. U. Kirss, P. P. Deutsch, S. I. Hommeltoft, R. Eisenberg, J. Bargon, R. G. Lawler, A. L. Balch, *J. Am. Chem. Soc.* **1987**, *109*, 8089–8091.
[23] R. W. Adams, J. A. Aguilar, K. D. Atkinson, M. J. Cowley, P. I. P. Elliott, S. B. Duckett, G. G. R. Green, I. G. Khazal, J. López-Serrano, D. C. Williamson, *Science* **2009**, *323*, 1708–1711.
[24] O. G. Salnikov, D. B. Burueva, I. V. Skovpin, I. V. Koptyug, *Mendeleev Commun.* **2023**, *33*, 583–596.
[25] A. B. Schmidt, C. R. Bowers, K. Buckenmaier, E. Y. Chekmenev, H. de Maissin, J. Eills, F. Ellermann, S. Glöggler, J. W. Gordon, S. Knecht, I. V. Koptyug, J. Kuhn, A. N. Pravdivtsev, F. Reineri, T. Theis, K. Them, J.-B. Hövener, *Anal. Chem.* **2022**, *94*, 479–502.
[26] F. Ellermann, P. Saul, J.-B. Hövener, A. N. Pravdivtsev, *Anal. Chem.* **2023**, *95*, 6244–6252.
[27] D. A. Barskiy, S. Knecht, A. V. Yurkovskaya, K. L. Ivanov, *Prog. Nucl. Magn. Reson. Spectrosc.* **2019**, *114–115*, 33–70.
[28] R. W. Adams, S. B. Duckett, R. A. Green, D. C. Williamson, G. G. R. Green, *J. Chem. Phys.* **2009**, *131*, 194505.
[29] K. X. Moreno, K. Nasr, M. Milne, A. D. Sherry, W. J. Goux, *J. Magn. Reson.* **2015**, *257*, 15–23.
[30] N. Eshuis, B. J. A. Van Weerdenburg, M. C. Feiters, F. P. J. T. Rutjes, S. S. Wijmenga, M. Tessari, *Angew. Chem., Int. Ed.* **2015**, *54*, 1481–1484.
[31] N. V. Chukanov, R. V. Shchepin, S. M. Joshi, M. S. H. Kabir, O. G. Salnikov, A. Svyatova, I. V. Koptyug, J. G. Gelovani, E. Y. Chekmenev, *Chem. – A Eur. J.* **2021**, *27*, 9727–9736.
[32] K. MacCulloch, A. Browning, P. TomHon, S. Lehmkuhl, E. Y. Chekmenev, T. Theis, *Anal. Chem.* **2023**, *95*, 7822–7829.
[33] W. Iali, P. J. Rayner, A. Alshehri, A. J. Holmes, A. J. Ruddlesden, S. B. Duckett, *Chem. Sci.* **2018**, *9*, 3677–3684.
[34] W. Iali, S. S. Roy, B. J. Tickner, F. Ahwal, A. J. Kennerley, S. B. Duckett, *Angew. Chem., Int. Ed.* **2019**, *58*, 10271–10275.
[35] I. Adelabu, J. Ettedgui, S. M. Joshi, S. Nantogma, M. R. H. Chowdhury, S. McBride, T. Theis, V. R. Sabbasani, M. Chandrasekhar, D. Sail, K. Yamamoto, R. E. Swenson, M. C. Krishna, B. M. Goodson, E. Y. Chekmenev, *Anal. Chem.* **2022**, *94*, 13422–13431.
[36] P. J. Rayner, M. J. Burns, A. M. Olaru, P. Norcott, M. Fekete, G. G. R. Green, L. A. R. Highton, R. E. Mewis, S. B. Duckett, *Proc. Natl. Acad. Sci. U. S. A.* **2017**, *114*, E3188–E3194.
[37] T. Theis, M. Truong, A. M. Coffey, E. Y. Chekmenev, W. S. Warren, *J. Magn. Reson.* **2014**, *248*, 23–26.
[38] S. Knecht, A. S. Kiryutin, A. V. Yurkovskaya, K. L. Ivanov, *Mol. Phys.* **2019**, *117*, 2762–2771.
[39] T. Theis, M. L. Truong, A. M. Coffey, R. V. Shchepin, K. W. Waddell, F. Shi, B. M. Goodson, W. S. Warren, E. Y. Chekmenev, *J. Am. Chem. Soc.* **2015**, *137*, 1404–1407.
[40] M. L. Truong, T. Theis, A. M. Coffey, R. V. Shchepin, K. W. Waddell, F. Shi, B. M. Goodson, W. S. Warren, E. Y. Chekmenev, *J. Phys. Chem. C* **2015**, *119*, 8786–8797.
[41] A. N. Pravdivtsev, I. V. Skovpin, A. I. Svyatova, N. V. Chukanov, L. M. Kovtunova, V. I. Bukhtiyarov, E. Y. Chekmenev, K. V. Kovtunov, I. V. Koptyug, J.-B. Hövener, *J. Phys. Chem. A* **2018**, *122*, 9107–9114.
[42] J. F. P. Colell, A. W. J. Logan, Z. Zhou, R. V. Shchepin, D. A. Barskiy, G. X. Ortiz, Jr., Q. Wang, S. J. Malcolmson, E. Y. Chekmenev, W. S. Warren, T. Theis, *J. Phys. Chem. C* **2017**, *121*, 6626–6634.
[43] A. S. Kiryutin, A. V. Yurkovskaya, P. A. Petrov, K. L. Ivanov, *Magn. Reson. Chem.* **2021**, *59*, 1216–1224.
[44] D. A. Barskiy, R. V. Shchepin, A. M. Coffey, T. Theis, W. S. Warren, B. M. Goodson, E. Y. Chekmenev, *J. Am. Chem. Soc.* **2016**, *138*, 8080–8083.
[45] O. G. Salnikov, N. V. Chukanov, A. Svyatova, I. A. Trofimov, M. S. H. Kabir, J. G. Gelovani, K. V. Kovtunov, I. V. Koptyug, E. Y. Chekmenev, *Angew. Chem., Int. Ed.* **2021**, *60*, 2406–2413.
[46] W. Iali, G. A. I. Moustafa, L. Dagys, S. S. Roy, *Magn. Reson. Chem.* **2021**, *59*, 1199–1207.
[47] K. Nepali, H.-Y. Lee, J.-P. Liou, *J. Med. Chem.* **2019**, *62*, 2851–2893.
[48] K. Hendrickson, M. Phillips, W. Smith, L. Peterson, K. Krohn, J. Rajendran, *Radiother. Oncol.* **2011**, *101*, 369–375.
[49] S. Kizaka-Kondoh, H. Konse-Nagasawa, *Cancer Sci.* **2009**, *100*, 1366–1373.
[50] P. Wardman, *Br. J. Radiol.* **2019**, *92*, 20170915.
[51] D. J. Thomson, N. J. Slevin, H. Baines, G. Betts, S. Bolton, M. Evans, K. Garcez, J. Irlam, L. Lee, N.

Melillo, H. Mistry, E. More, C. Nutting, J. M. Price, S. Schipani, M. Sen, H. Yang, C. M. West, E. Aynsley, R. Banner, G. Barnett, K. Cardale, J. Christian, L. Fresco, W. Grant, A. Hartley, J. Lester, P. McCloskey, R. Prestwich, A. Shenoy, S. Thiagarajan, K. Wood, *Int. J. Radiat. Oncol.* **2023**, DOI: 10.1016/j.ijrobp.2023.11.055.

[52] J. M. Henk, K. Bishop, S. F. Shepherd, *Radiother. Oncol.* **2003**, *66*, 65–70.

[53] D. O. Guarin, S. M. Joshi, A. Samoilenko, M. S. H. Kabir, E. E. Hardy, A. M. Takahashi, J. H. Ardenkjaer-Larsen, E. Y. Chekmenev, Y. Yen, *Angew. Chem., Int. Ed.* **2023**, *62*, e202219181.

[54] R. V. Shchepin, J. R. Birchall, N. V. Chukanov, K. V. Kovtunov, I. V. Koptyug, T. Theis, W. S. Warren, J. G. Gelovani, B. M. Goodson, S. Shokouhi, M. S. Rosen, Y. F. Yen, W. Pham, E. Y. Chekmenev, *Chem. – A Eur. J.* **2019**, *25*, 8829–8836.

[55] J. R. Birchall, M. S. H. Kabir, O. G. Salnikov, N. V. Chukanov, A. Svyatova, K. V. Kovtunov, I. V. Koptyug, J. G. Gelovani, B. M. Goodson, W. Pham, E. Y. Chekmenev, *Chem. Commun.* **2020**, *56*, 9098–9101.

[56] A. S. Kiryutin, A. V. Yurkovskaya, K. L. Ivanov, *ChemPhysChem* **2021**, *22*, 1470–1477.

[57] M. Fekete, F. Ahwal, S. B. Duckett, *J. Phys. Chem. B* **2020**, *124*, 4573–4580.

[58] S. Nantogma, M. R. H. Chowdhury, M. S. H. Kabir, I. Adelabu, S. M. Joshi, A. Samoilenko, H. de Maissin, A. B. Schmidt, P. Nikolaou, Y. A. Chekmenev, O. G. Salnikov, N. V. Chukanov, I. V. Koptyug, B. M. Goodson, E. Y. Chekmenev, *Anal. Chem.* **2024**, DOI: 10.1021/acs.analchem.3c05233.

[59] J. W. Blanchard, B. Ripka, B. A. Suslick, D. Gelevski, T. Wu, K. Münnemann, D. A. Barskiy, D. Budker, *Magn. Reson. Chem.* **2021**, *59*, 1208–1215.

[60] O. Semenova, P. M. Richardson, A. J. Parrott, A. Nordon, M. E. Halse, S. B. Duckett, *Anal. Chem.* **2019**, *91*, 6695–6701.

[61] D. A. Barskiy, K. V. Kovtunov, I. V. Koptyug, P. He, K. A. Groome, Q. A. Best, F. Shi, B. M. Goodson, R. V. Shchepin, A. M. Coffey, K. W. Waddell, E. Y. Chekmenev, *J. Am. Chem. Soc.* **2014**, *136*, 3322–3325.

[62] S. Knecht, S. Hadjiali, D. A. Barskiy, A. Pines, G. Sauer, A. S. Kiryutin, K. L. Ivanov, A. V. Yurkovskaya, G. Buntkowsky, *J. Phys. Chem. C* **2019**, *123*, 16288–16293.

[63] R. V. Shchepin, L. Jaigirdar, T. Theis, W. S. Warren, B. M. Goodson, E. Y. Chekmenev, *J. Phys. Chem. C* **2017**, *121*, 28425–28434.

[64] L. S. Lloyd, A. Asghar, M. J. Burns, A. Charlton, S. Coombes, M. J. Cowley, G. J. Dear, S. B. Duckett, G. R. Genov, G. G. R. Green, L. A. R. Highton, A. J. J. Hooper, M. Khan, I. G. Khazal, R. J. Lewis, R. E. Mewis, A. D. Roberts, A. J. Ruddlesden, *Catal. Sci. Technol.* **2014**, *4*, 3544–3554.

[65] S. A. Dingsdag, N. Hunter, *J. Antimicrob. Chemother.* **2018**, *73*, 265–279.

[66] L. D. Vázquez-Serrano, B. T. Owens, J. M. Buriak, *Chem. Commun.* **2002**, *21*, 2518–2519.

TOC Graphics: